ACS Catalysis

Research Article

pubs.acs.org/acscatalysis

Selective Heterogeneous CO_2 Electroreduction to Methanol

Seoin Back,[†] Heejin Kim,[†,‡] and Yousung Jung*[,†]

[†]Graduate School of EEWS, Korea Advanced Institute of Science and Technology (KAIST), 335 Gwahangno, Yuseong-gu, Daejeon 305-701, Republic of Korea

[‡]Analysis Research Division, Suncheon Center, Korea Basic Science Institute, Suncheon 540-742, Republic of Korea

Supporting Information

ABSTRACT: Catalytic electroreduction of carbon dioxide to useful chemical feedstocks is an environmentally and technologically important process, yet the low energy efficiency and difficulty in controlling product selectivity are great challenges. The reason for part of the latter is that there are presently no catalyst design principles to selectively control CO_2 electroreduction toward a desired product. In this work, as a first attempt, we suggest combining a few criteria (CO binding energy, OH binding energy, and H binding energy) that can be collectively used as activity- and selectivity-determining descriptors to preferentially produce methanol over methane from CO_2 electroreduction. We then apply these concepts to near-surface alloys (NSAs) to propose efficient and selective CO_2 electrochemical reduction catalysts to produce methanol. The W/Au alloy is identified as a promising candidate to have increased catalyst efficiency (decreased CO_2 reduction overpotential and increased overpotential for unwanted hydrogen evolution) as well as improved product selectivity toward methanol, in comparison to conventional Cu catalyst.

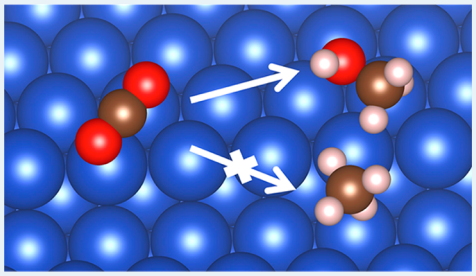

KEYWORDS: *density functional calculations, methanol production, CO_2 electroreduction, computational screening, near-surface alloys, surface chemistry, electrocatalysts*

INTRODUCTION

For past decades, significant attention has been paid to the electroreduction of CO_2 as a sustainable means to utilize CO_2 after capture in order to address global climate challenges.[1,2] The electrochemical conversion of CO_2 into various chemicals has particular advantages as follows: (1) the reaction is feasible under ambient temperature and pressure, implying that the cost of capital investment and operation is low; (2) since the process essentially converts electrical energy into chemical energy, it can be useful to store energy generated from the renewable sources; (3) the reaction products are numerous, many of which are industrially important feedstocks such as methane, carboxylic acid, carbon monoxide, alcohols, and even longer hydrocarbon chains.[3−6] Despite these advantages, high activation barrier or large overpotential (low energy efficiency) and poor product selectivity are the two main obstacles for practical applications of electroreduction of CO_2 at present.

At least 16 different CO_2 reduction products have been identified,[7] among which the more dominant products are shown in eqs 2−8 with the associated reduction potentials (E_0) relative to the standard hydrogen electrode (SHE) (eq 1).[3] A more positive E_0 indicates that the reaction is more favorable thermodynamically according to the relationship $\Delta G = -nFE_0$, where n is the number of electrons transferred during the redox reaction and F is the Faraday constant. On the basis of E_0, it is thus seen that the CO_2 reductions toward hydrocarbon or alcohol products (eq 5−8) should actually be thermodynamically more favorable than the CO, HCOOH, CH_2O and hydrogen productions (eq 1−4), which have a positive free energy of reaction. Experimentally, however, the small molecules (CO, HCOOH, and H_2) that involve the transfer of at most two electrons were primarily observed at most electrocatalytic electrodes. This observation is attributed to the slow kinetics of multiple electron (beyond $n = 2$) transfer such as in the reaction products of eq 4−8. It is observed, however, that Cu can produce various hydrocarbons (methane being a major and the simplest such product with $n = 8$) with moderate current density.[8,9]

$$2H^+ + 2e^- = H_2 \quad E_0 = -0.000\ V_{SHE} \tag{1}$$

$$CO_2(g) + 2H^+ + 2e^- = HCOOH(l) \quad E_0 = -0.250\ V_{SHE} \tag{2}$$

$$CO_2(g) + 2H^+ + 2e^- = CO(g) + H_2O(l) \quad E_0 = -0.106\ V_{SHE} \tag{3}$$

$$CO_2(g) + 4H^+ + 4e^- = CH_2O(l) + H_2O(l) \quad E_0 = -0.070\ V_{SHE} \tag{4}$$

$$CO_2(g) + 6H^+ + 6e^- = CH_3OH(l) + H_2O(l) \quad E_0 = 0.016\ V_{SHE} \tag{5}$$

$$CO_2(g) + 8H^+ + 8e^- = CH_4(g) + 2H_2O(l) \quad E_0 = 0.169\ V_{SHE} \tag{6}$$

$$CO_2(g) + 12H^+ + 12e^- = C_2H_4(g) + 4H_2O(l) \quad E_0 = 0.064\ V_{SHE} \tag{7}$$

$$CO_2(g) + 12H^+ + 12e^- = C_2H_5OH(l) + 3H_2O(l) \quad E_0 = 0.084\ V_{SHE} \tag{8}$$

Received: October 15, 2014
Revised: December 22, 2014
Published: December 23, 2014

DOI: 10.1021/cs501600x
ACS Catal. 2015, 5, 965−971

One of the more desired C-1 hydrocarbon products from CO_2 reduction is methanol rather than methane, since methanol can be used as a liquid fuel for direct methanol fuel cells (DMFCs) and modified diesel engines.[10,11] Indeed, most methanol today is produced from methane through syngas.[12] Despite such an industrial importance of direct and selective production of methanol from CO_2, only a few heterogeneous catalysts have been investigated for converting CO_2 to methanol.[13] In addition, theoretical studies have focused mainly on the design of catalysts for methane production with reduced overpotential,[14−17] rather than for methanol. In this work, we propose a method to design electrochemical catalysts for converting the CO_2 into alcohols (methanol) over hydrocarbons (methane) by finding a descriptor that determines the selectivity.

A Cu electrode has been known to produce various hydrocarbons and alcohols from CO_2.[18] It has been suggested that the crystal orientation plays a significant role in determining products. Experimentally, CH_4 production is favored at (111) facets and steps, while C_2H_4 production is favored at (100) facets.[19,20] Recently, Nørskov and co-workers showed that the stepped surface of Cu such as (211) is more active than other facets toward the electroreduction of CO_2 to hydrocarbons[21] with the help of density functional theory (DFT) calculations.[14,22] They suggested reaction mechanisms for the Cu (211) surface in which the potential-determining step (PDS) is the protonation of adsorbed CO to form CHO species ($*CO + H^+ + e^- \rightarrow *CHO$, where * denotes the surface-adsorbed species), which is also supported by experiments that *CHO is the key intermediate toward the formation of methane.[22,23] Also, the authors showed that there is a volcano relationship between the surface binding energy of CO (as a representative of adsorbates binding to the surface through carbon such as COOH, CO, CHO, and CH_2O) and the associated reaction overpotential.[14] This activity volcano plot as a function of the CO binding affinity, namely CO-analogous volcano, suggests that the PDS is the protonation of *CO to form *CHO for the strong CO binding surfaces (left leg of volcano), whereas the protonation of CO_2 to form *COOH is the PDS for the weak CO binding surfaces (right leg of volcano). According to these theoretical analyses, better catalysts should have a slightly weaker binding of CO than the Cu electrode to approach the top of the volcano: i.e., minimized overpotential. Nevertheless, a similar trend in binding energies of *CHO and *CO that scale with a slope close to 1 imposes a great difficulty for designing catalysts better than Cu in practice.[14]

Nørskov and co-workers also considered OH binding (as a representative of adsorbates binding to the surface through oxygen such as OCH_3, O, and OH) and constructed a similar OH-analogous volcano plot. However, the results indicated that elementary steps which involve the adsorption of O-bound species in the OH-analogous volcano exhibit much smaller overpotentials in comparison to the C-bound intermediates in the CO-analogous volcano. That is, the CO binding energy alone can be used as a proper descriptor to find an optimal CO_2 electrocatalyst for methane production, as long as the materials do not have extremely weak or strong OH affinities. If the focus, however, is the selective production of methanol (rather than methane) as in the present case, the reaction intermediates that bind through oxygen such as OH should be the key species, since their binding strength will determine the fate of $*OCH_3$ to further reduce to form either CH_3OH (desired product) or CH_4 (byproduct).

In this study, therefore, we introduce the OH binding energy as a descriptor that determines the selectivity between CH_3OH and CH_4 for electroreduction of CO_2. We then apply this concept to near-surface alloys (NSAs) to design new alloy catalysts for the CO_2 electroreduction to methanol with both enhanced activity and selectivity in comparison to those of Cu. Since Cu is already near the top of the activity volcano, the tuning of surface reactivity should be quite delicate and fine to provide the optimal binding energy of CO for further reduced overpotential. In this point of view, bimetallic NSAs are promising, since they can offer a quasi-continuous spectrum of binding energies by systematically altering the combination of alloying elements to find the alloy couple with the optimal binding energy.[24]

COMPUTATIONAL DETAILS

Calculation Models. There are two types of ideal NSAs, "overlayer" and "subsurface" configurations, depending on the position of the secondary alloying metal layer, as illustrated in Figure 1. While the bimetallic NSAs can be composed of

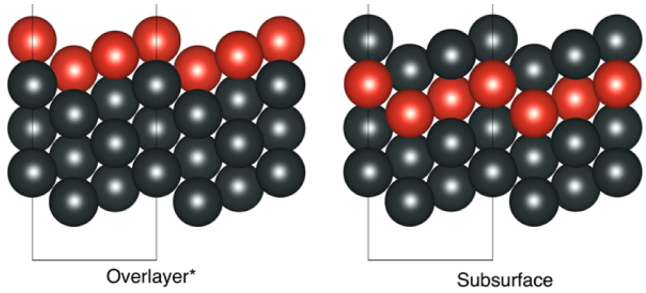

Figure 1. Schematics for (211) stepped overlayers (A*/B) and subsurface (A/B) alloys. Red and black atoms denote the solute (A) and host (B) metals, respectively.

diverse metal elements, the practical combination of metal species and their configurations (overlayer or subsurface) are determined by the thermodynamic stability. We chose Cu, Pt, Pd, Ag, and Au as host metals since Cu, which has an intermediate CO binding, is currently the most promising element at the top of the volcano, while the Pt and Pd group and Au and Ag group are well-known as having strong and weak CO binding surfaces, respectively, and hence can be considered as representatives of each character. Various alloying solute metals, including Ag, Au, Cu, Ir, Os, Pd, Pt, Re, Rh, Ta, V, W, and Zn, are considered. We evaluated the relative stability of the two equilibrium configurations (overlayer or subsurface) of NSAs under vacuum conditions by comparing the formation energy of two configurations (Figure S1, Supporting Information). We note that both overlayer and subsurface NSAs were successfully synthesized experimentally. An electrodeposition of Cu on Pt (111) yielded the Cu overlayer NSA, and consecutive annealing under an H_2 atmosphere yielded the Cu subsurface NSA.[25] In addition, a Cu/Pt (211) overlayer was also synthesized by the electrodeposition of Cu on a Pt (211) surface.[26]

The outermost surface configuration of alloys may become complicated when gas molecules such as CO, O_2, and N_2 are present in the ambient environment, since their binding affinity toward each metal surface is largely different, thus altering the

DOI: 10.1021/cs501600x
ACS Catal. 2015, 5, 965−971

surface morphology of alloys. In recent experiments, Varela et al. successfully deposited Cu overlayers on Pt (111) and Pt (211) surfaces, but the buried Pt atoms get exposed in the presence of CO, since the strong interaction between CO and Pt destabilizes the covering of Cu overlayers.[26] This result indicates that the stability of NSA-based catalysts should also be considered in the presence of possible intermediate adsorbate species. The latter consideration of the alloy stability upon gas adsorption will reduce the possible number of solute/host combinations for further evaluation of catalytic activity and selectivity. The stability analysis toward various reaction intermediates is presented in Figures S2 and S3 and Supplementary Note 1 (Supporting Information). We considered NSAs with a pure metal surface, which are selected on the basis of the stability conditions as shown in the Supporting Information, to understand the trends of catalytic activity and selectivity as a function of alloying elements. Structural defects and coverage of adsorbates that may alter the catalytic behaviors are not considered here for simplicity, but we expect that the systematic comparison of alloying elements in this work still provide the key guiding principle for the design of bimetallic NSAs.

Theoretical Methods. We performed spin-polarized density functional theory (DFT)[27] calculations using the Vienna ab initio Simulation Package (VASP).[28,29] The revised Perdew–Burke–Ernzerhof (RPBE)[30,31] exchange-correlation functional of the generalized gradient approximation (GGA) was used with the projector-augmented wave (PAW) pseudopotential.[32] A plane-wave cutoff energy of 500 eV was used for all geometry optimizations. Overlayers and subsurface alloys in (211) stepped geometry were fully optimized until the residual force was less than 0.05 eV/Å without any constraints. For calculating adsorption energies and for validating stabilities of alloys by calculating migration energies, the bottom two layers were fixed to their optimized positions of the slab without adsorbates, while the upper two layers and adsorbates were fully relaxed. K points were sampled using a 3 × 2 × 1 Monkhorst–Pack mesh,[33] reciprocally proportional to the lattice parameters. Our four-layer slab models contain 48 atoms with a slab size of 3 × 4 × 4, spaced more than approximately 15 Å to avoid an imaginary interaction between periodic images.

The adsorption energies of adsorbates are defined as

$$E_{CxHyOz} = E_{slab+C_xH_yO_z} - E_{slab} - xE_C - yE_H - zE_O$$

where $E_{slab+C_xH_yO_z}$, E_{slab}, E_C, E_H, and E_O are the energy of the total system, the energy of the clean slab, and the energies of C, H, and O atoms, respectively. The energies of C, H, and O atoms are referenced to graphene, gaseous hydrogen (H_2), and the difference between water and hydrogen ($H_2O - H_2$), respectively. For stable adsorbates, such as CH_2O and CO, energies of molecules were calculated in a large periodic box. To correct the inconsistency between theoretical and experimental gas-phase reaction enthalpies, +0.45 eV is added to the total energy of CO_2, which has a −OCO− backbone, as found in the previous study.[22]

Free energy corrections at 18.5 °C, including the zero-point energies and entropies, are taken from the previous DFT studies of CO_2 electroreduction on Cu (211) surfaces.[14,22] In the previous DFT calculations, placing a hexagonal water layer on the Pt (111) surface stabilized the *OH (direct binding of *OH to the surface) and *OOH (indirect binding of *OH through other atoms) species by approximately 0.5 and 0.25 eV, respectively.[34−37] The same procedure for the Cu (111) surface yielded the stabilization of both *CO and *CHO by approximately 0.1 eV by the presence of water.[22] Since the explicit treatment of solvation effects is computationally too demanding, we used these approximate solvation effects in this study. In reference to the chemical potential of the proton and electron pair, which is known as the computational hydrogen electrode (CHE),[34] one can build a free energy diagram and estimate a limiting potential. CHE assumes that the chemical potential of a proton–electron pair ($\mu[H^+ + e^-]$) is in equilibrium with that of hydrogen ($\mu[H_2]$) at 0 V, 101325 Pa of H_2, and all pH values and temperatures. As an external potential (U) is applied, the chemical potential of the proton–electron pair is shifted by $-eU$; therefore, $\mu[H^+ + e^-] = \mu[H_2] - eU$.

The chemical potential of the proton–electron pair leads to the limiting potential (U_L) for each proton–electron transfer reaction and the whole CO_2 reduction reaction. The limiting potential for each proton–electron transfer step is the least negative potential to make the reaction path thermodynamically exergonic (downhill) and is defined by $U_L = -\Delta G^{0\,V}/e$, where $\Delta G^{0\,V}$ is the Gibbs energy change of the proton–electron transfer step at zero electrode potential. Therefore, $\Delta G = 0$ at $U = U_L$. Similarly, the limiting potential for the whole reaction is defined by the potential needed to make the overall reaction exergonic (all downhill), $U_L = -\Delta G^{0\,V}_{max}/e$, where $\Delta^{0\,V}_{max}$ is the largest positive change in free energy among all proton–electron transfer steps involved at zero electrode potential. We note that the "limiting potential" defined and used here is different from the onset potential measured in electrochemical studies, where the onset potential is rather arbitrary as to what current density is used to define the onset.

Our investigation focuses on the thermodynamic stability of reaction intermediates, which is a required but not necessarily sufficient condition for predicting catalytic reactions. The reaction may occur slowly if the kinetic barriers of intermediate reactions (proton–electron transfer) are significantly higher than 0.7 eV, for example, which might be a surmountable barrier under ambient temperature.[22,38] On the other hand, the previous measurement of current densities of CO_2 electroreduction by Cu indicated a significant activity increase (from 0.1 to 1 mA/cm^2) with the external potential varying from −0.5 to −0.8 V,[8] indicating that the kinetic barriers for all proton–electron transfer reactions become surmountable with an increase in the external potential (more negative). In addition, the previous DFT calculations showed that the proton transfer barrier in the solution phase is as low as 0.3 eV on the metal catalyst, although the barrier in the vapor phase was significantly higher, 1.1 eV.[39] Furthermore, according to the Brønsted–Evans–Polanyi (BEP) relation, the kinetic barrier decreases when the reaction energy becomes more exothermic,[40−42] suggesting that the negative external potential, which makes the CO_2 electoreduction reaction more exothermic, can reduce the intrinsic kinetic barriers. On these basis, we expect that the thermodynamic consideration of CO_2 electroreduction can indeed provide a valuable guideline for predicting the electrochemical catalytic activities.

RESULTS AND DISCUSSION

As a means to define the catalysts activity and selectivity for improved CO_2 reduction reaction toward methanol production, we use the following three criteria. (1) As suggested by

DOI: 10.1021/cs501600x
ACS Catal. 2015, 5, 965−971

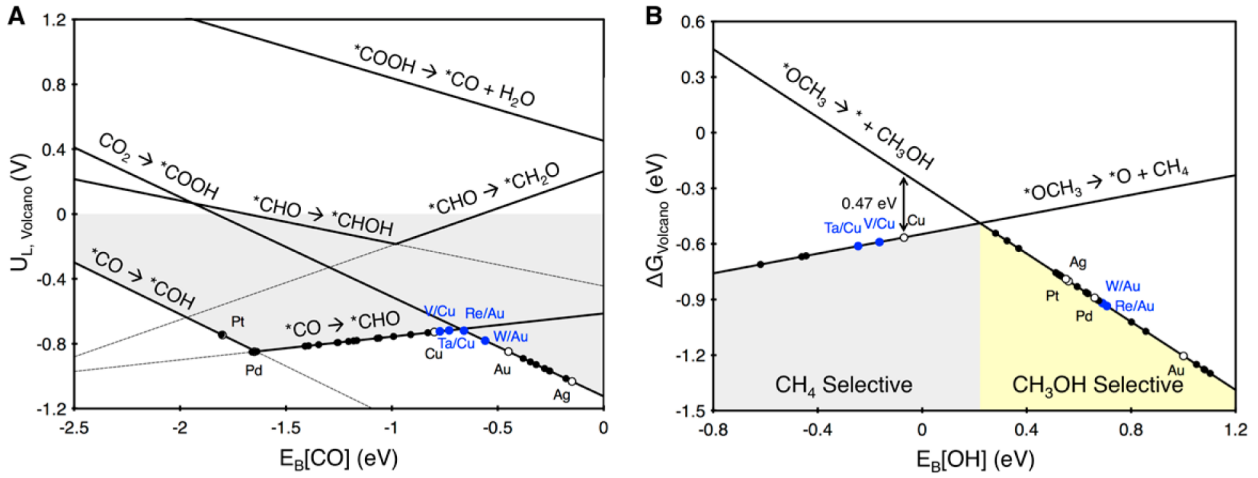

Figure 2. (A) Predicted limiting potential ($U_{L,Volcano}$) for the elementary CO_2 electroreduction steps that involve the intermediates binding through carbon. (B) Predicted Gibbs free energy changes in the selectivity-determining step (CH_4 vs CH_3OH production) as a function of OH binding energy at zero electrode potential. The CH_3OH production is preferred at weaker (less negative) OH binding energies. Out of total 27 stable NSAs calculated in this study, those NSAs that are located close to the top of CO-analogous volcano (i.e., between Cu and Au) are marked in blue, while other NSAs and pure metals are marked in black (also calculated in this study). Note that the PDS, actual calculated U_L, and reduction products for all NSAs are included in Table S4 (Supporting Information) for comparison, where the difference between the predicted and actual limiting potentials is within approximately 0.1 V. We note that this volcano is usually semiqualitative in guiding the design of new catalysts, given a scatter in scaling relations.

Peterson and Norskov,[14] optimal catalysts should have an optimal CO binding energy, which is the limiting potential determining descriptor. (2) To minimize the unwanted hydrogen evolution competing reaction (HER), the new catalysts should have as weak an H adsorption energy as possible to suppress the HER by increasing the reaction overpotential.[43] (3) The selectivity of methanol production over methane during electroreduction can be determined by utilizing the OH binding energy. That is, the catalyst surfaces that weakly bind the OH species can selectively produce CH_3OH by easy removal of the $-OCH_3$ group from the surface ($*OCH_3 + H^+ + e^- \rightarrow * + CH_3OH$), whereas the catalysts with strong OH binding favor the methane production after the breaking of the $*O-CH_3$ bond ($*OCH_3 + H^+ + e^- \rightarrow *O + CH_4$), as shown in Figure 2B. The rationalization of these three conditions and the results are described below in more detail.

Optimal CO Binding (Desired Reduction Reaction). Previous theoretical studies revealed that binding energies of reaction intermediates are correlated within the 0.1−0.2 eV error;[14,44−46] that is, the surface binding energies of various reaction intermediates are correlated by certain scaling relationships.[47−49] We find that the present CO binding energy vs activity plot established on the stable NSAs (Figure 2A) shows a volcano behavior similar to that of Peterson,[14] supporting the generality of the scaling and volcano relations on transition-metal surfaces. That is, either protonation of CO_2 to form *COOH or protonation of *CO to form *CHO is the PDS, except for the too strong CO binding region (E_B[CO] < −1.6 eV), where the protonation of *CO to form *COH is the PDS. We expect that this similar volcano behavior is attributed to the ideal surface model of NSAs that consists of pure metals, as in the previous study.[14] For the present construction, a catalyst with a CO binding energy of −0.67 eV exhibits the lowest overpotential (Figure 2A), similar to the −0.60 eV of previously calculated optimal CO binding.[14] The slight shift of the volcano top is perhaps due to the inclusion of a large number of NSAs as well as pure metals (total of 32 surfaces), while the previous study considered only 7 pure metals.[14]

Optimal H Binding (Unwanted Competing Reduction). The competing HER can hinder the desired CO_2 reduction, since the thermodynamic equilibrium potential of the HER is less negative (more favorable) than that of the CO_2 reduction reaction.[8] Such unwanted HER can be suppressed by increasing the reaction overpotential. For that, one can use the volcano plot, but in this case the catalyst needs to be as far away from the volcano top as possible to maximize the reaction overpotentia: i.e., either very strong binding or very weak binding for the hydrogen atom is desirable. In a previous theoretical study, Chan et al. similarly suggested that the difference in the limiting potentials between the CO_2 electroreduction reaction and HER ($U_L(CO_2) - U_L(H_2)$) plotted versus CO_2 limiting potential ($U_L(CO_2)$) determines the selectivity of the CO_2 reduction over HER.[15] Nevertheless, we expect that the weak H binding catalysts are more suitable than the strong H binding catalysts, as have been tested for metal-functionalized porphyrin-like graphene[50] and intermetallic alloys.[16] If the H binding is too strong, it can stick to the surface and reduce the number of active sites for reaction. Furthermore, the binding energy of H is known to decrease with an increase in the surface coverage of H atoms,[46,51] indicating that the reaction overpotential is lowered to enhance the HER at high coverage conditions. Therefore, in this study, we propose that an ideal CO_2 reduction catalyst should maintain relatively weak hydrogen binding to compete against HER.

Optimal OH Binding (Product Selectivity toward CH_3OH against CH_4). In the proposed reaction mechanism, the selectivity of either CH_3OH or CH_4 is determined by the relative strength of the surface $(*)-OCH_3$ bond in comparison to the $*O-CH_3$ bond. A weaker interaction between O and the surface would preferentially produce CH_3OH by facilitating the desorption of a whole $*OCH_3$ group from the surface, while a strong interaction between O and the surface would provide more chances to break the $O-CH_3$ bond, producing CH_4 as a main product in the next protonation step. In such considerations of interaction between O and the metal surface,

DOI: 10.1021/cs501600x
ACS Catal. 2015, 5, 965−971

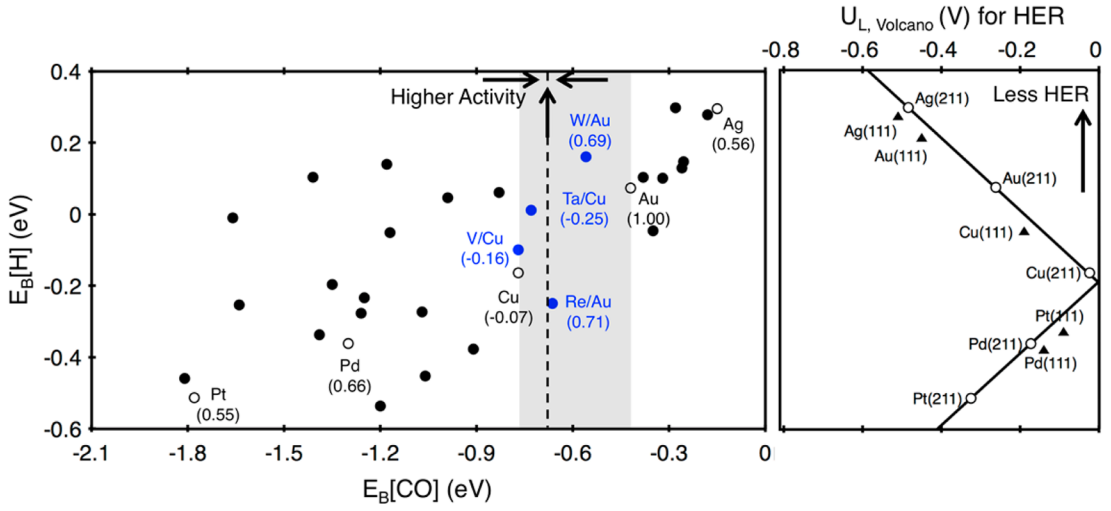

Figure 3. CO and H binding energies for the lowest energy configurations of NSAs (black dots), potentially promising NSAs (blue dots) with low expected overpotentials (those that are between Cu and Au), and pure metals (hollow black dots). The values in parentheses are the OH binding energies. Binding energies of other NSAs are shown in Table S3 (Supporting Information). The vertical dashed line indicates the optimal CO binding energy: i.e., the top of the volcano in Figure 2A. On the right, the volcano relation of the limiting potential ($U_{L,Volcano}$, x axis) for the hydrogen evolution reaction is shown as a function of H binding energies (y axis). The arrows indicate a desired direction for catalyst design with higher activity for CO_2 reduction reaction as well as low HER. Hollow circles (calculated in this study) and black triangles (taken from ref 46) indicate the calculated overpotential for the HER reaction.

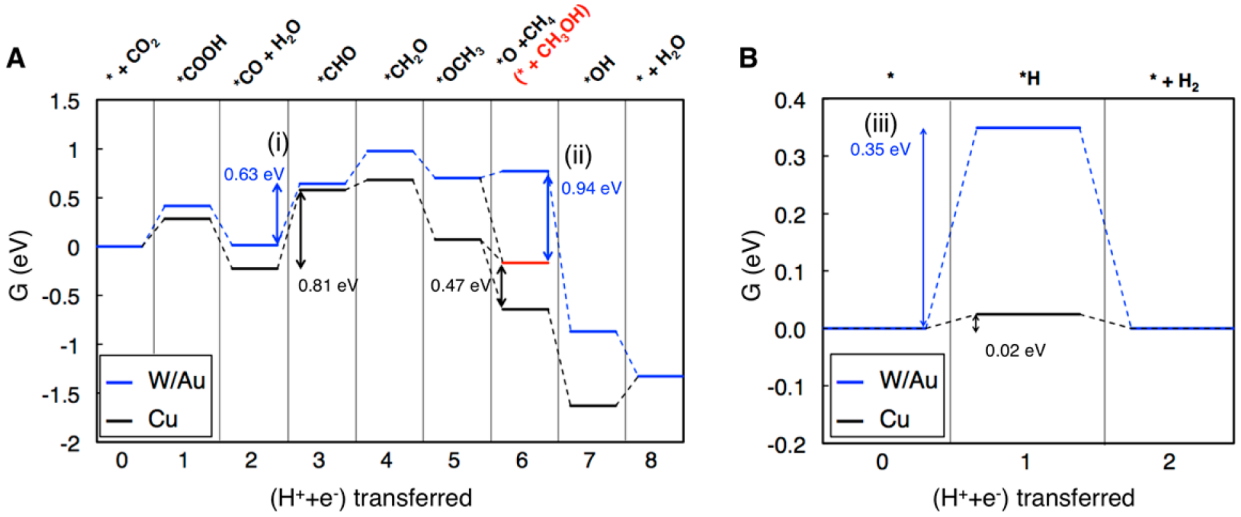

Figure 4. Free energy diagram for the (A) CO_2 electroreductions to CH_4 or CH_3OH (shown in red) and (B) H_2 evolution reactions at zero electrode potential (U = 0 V) for Cu (black) and W/Au (this work, blue). Each reaction step involves a proton−electron pair ($H^+ + e^-$) transferred from the solution to the electrode. The asterisk alone represents a clean slab, while *CO, for example, represents the CO-adsorbed surface. Three key points that are discussed in the main text are indicated as i−iii in the figure: (i) overpotential of the CO_2 reduction reaction, (ii) selectivity between CH_4, and CH_3OH, and (iii) overpotential of the H_2 evolution reaction.

we can use an OH binding energy as a descriptor due to the scaling relation in binding energies among OH analogous species. Figure 2B shows the Gibbs free energy changes of two important reaction steps that determine the selectivity ($*OCH_3 \rightarrow CH_3OH$ vs $*OCH_3 \rightarrow *O + CH_4$) as a function of OH binding energy for 27 NSAs and 5 pure metal surfaces. The production of CH_4 and CH_3OH are respectively preferred in the left-side and right-side surfaces of the figure. For example, the Cu (211) surface has a thermodynamic preference of CH_4 over CH_3OH by 0.47 eV, as marked with an arrow in Figure 2B. It was indeed observed in electroreduction experiments that the polycrystalline Cu surface produces CH_4 as a major product over other alcohols.[18]

We note that it may be also possible for methanol to be produced via the formation of hydrated formaldehyde (CH_2O) or methanediol ($H_2C(OH)_2$).[52] However, considering an extremely small equilibrium pressure of desorbing CH_2O (2×10^{-11} Pa) at a limiting potential for the reduction of *CO to *CHO (−0.74 V vs RHE),[22] we expect that the methanediol pathway should be negligible in producing methanol. Similarly, at the latter external potential, the protonation step of the adsorbed formaldehyde ($*CH_2O$) to form $*OCH_3$ becomes substantially downhill thermodynamically, making the methanol production via $*OCH_3$ the most plausible reaction pathway.

Screening Near-Surface Alloys for Enhanced Activity and Selectivity. We applied the last three criteria (CO, H, and

DOI: 10.1021/cs501600x
ACS Catal. 2015, 5, 965−971

OH binding energies) to find a catalyst better than Cu for producing the CH_3OH among the NSAs. Figure 3 is the CO binding energy vs H binding energy for NSAs that are calculated to be stable without significant mixing (Figure S3, Supporting Information). The OH binding energy is also presented in parentheses. Among these NSAs, on the basis of the three criteria described above, the W/Au subsurface alloy is identified to be a promising candidate: its CO binding energy is close to the optimal value and it has weak H and OH binding energies, leading to a high selectivity toward CH_3OH production. Although the Re/Au, Ta/Cu, and V/Cu alloys have more appropriate CO binding energies than Cu or W/Au, their H binding energies are not weak enough to ensure the large overpotential to suppress HER. In particular, the subsurface Re/Au exhibits a minimized reduction overpotential (Figures 2A and 3) and a high selectivity toward methanol over methane (Figure 2B) among the NSAs tested here, but as shown in Figure 3, the lowest overpotential for HER will promote the consumption of protons and electrons for HER; thus, Re/Au is not suitable for producing CH_3OH. These examples highlight the importance and necessity of using all three criteria described above to design new catalysts that are both efficient and selective for methanol production.

Comparison of W/Au vs Cu. In Figure 4, we compare the free energy diagram for the W/Au subsurface alloy (the new catalyst designed here) and conventional Cu surfaces toward CO_2 electroreduction and H_2 evolution reactions. Three important points can be made clear as follows.

(i) For both catalysts, PDS is the third electron and proton transfer step (*CO → *CHO), but the calculated limiting potential for W/Au (−0.63 V) is smaller than that for Cu (−0.81 V). We note that the limiting potential of −0.81 V for Cu (211) in this work is in reasonable agreement with the previous result (−0.74 V).[22] The decrease of limiting potential by 0.18 V using W/Au corresponds to a 25% improvement in overall energy requirement for the electrochemical reaction in comparison to the current Cu electrode. This value is also comparable to that of the recently reported Cu_{55} nanoparticle on the defective graphene that has a limiting potential of −0.68 V.[17] We additionally evaluated the thermodynamics of the CO_2 chemisorption step (* + CO_2 → *CO_2) on Cu and W/Au surfaces, the very first adsorption step that is often neglected in the literature, to check whether the inclusion of this reaction changes the free energy diagram. The reaction free energy for this step is calculated to be −0.07 eV for both surfaces, leaving our conclusions (PDS and U_L) unchanged.

(ii) For the selectivity-determining step, i.e., the sixth proton and electron transfer in Figure 4A, the thermodynamic preference for CH_3OH over CH_4 is much larger for W/Au (0.94 eV) than for Cu (0.47 eV). These detailed free energy considerations are consistent with the experimental results that Cu produces CH_4 as a major product and validate the use of OH binding energy as a proper selectivity-determining descriptor described above.[18]

(iii) As discussed in Figure 3, the HER will be suppressed on the W/Au catalyst due to its weak E_B[H] value (0.16 eV for W/Au vs −0.16 and 0.07 eV for Cu and Au, respectively). Figure 4B compares the free energy to produce gaseous H_2 on W/Au vs Cu. The calculated limiting potential for HER on W/Au is −0.35 V, while that on Cu is −0.02 V. This increase in overpotential for HER on W/Au means that it is much less prone to produce H_2 using W/Au than with Cu, thereby enhancing the product selectivity by suppressing unwanted H_2 evolution. We note that the *OH removal step should also be considered for the catalysts with strong E_B[OH] when predicting U_L for HER. For instance, the calculated limiting potential for HER for Cu is −0.02 V, while the actual evolution of H_2 in experiments occurred at an overpotential higher than −0.02 V, which was attributed to the removal step of *OH to clear the active sites for H_2 evolution. For other metal catalysts (Ag, Au, and Pt), where the *OH removal is not a potential-determining step due to weak *OH binding, the calculated limiting potentials (−0.48, −0.26, and −0.09 V) and experimental HER activities (Pt > Au > Ag) are in good agreement.[46]

CONCLUSION

To select a catalyst for CO_2 electroreduction toward methanol with high efficiency and selectivity, we proposed to combine three criteria: one activity condition (CO binding energy) and two selectivity conditions (OH and H binding energies).

(1) The optimal CO binding energy (−0.67 eV) is desired to decrease the limiting potential for CO_2 electroreduction, whereas a weak H binding energy is desired to increase the limiting potential for unwanted HER. The catalysts satisfying these two conditions will have a high catalytic productivity with an efficient reduction of CO_2 and a high selectivity by suppressing HER.

(2) We introduce the OH binding energy as a selectivity-determining descriptor for CH_3OH vs CH_4 products, on the basis that the protonation of *OCH_3 is a key step in the formation of either alcohols or hydrocarbons. The catalyst with a weak OH binding will preferentially produce the methanol, while a strong binding will preferentially produce methane.

(3) Among the various NSAs screened, the W/Au alloy exhibits several advantages for methanol production in comparison to the existing Cu: (i) it has lower overpotential than Cu (−0.63 vs −0.81 V) for electroreduction of CO_2, (ii) it preferentially produces more valuable CH_3OH over CH_4, and (iii) it efficiently suppress the unwanted HER.

ASSOCIATED CONTENT

Supporting Information

The following file is available free of charge on the ACS Publications website at DOI: 10.1021/cs501600x.

Computational details and additional information on NSAs, including configurations, stability analysis of NSAs under reaction conditions, scaling relations between different intermediate binding energies, and E_B[CO], E_B[H], and E_B[OH] values for all NSAs, and a summary of the PDS, the calculated limiting potential, and CO_2 reduction products (PDF)

AUTHOR INFORMATION

Corresponding Author

*E-mail for Y.J.: ysjn@kaist.ac.kr.

Notes

The authors declare no competing financial interest.

ACKNOWLEDGMENTS

This research was supported by the Global Ph.D. Fellowship Program (S.B.) through the NRF funded by the Ministry of Education (NRF-2014H1A2A1016055) and KOREA CCS R&D Center (NRF-2014M1A8A1049252). The generous gift of supercomputing time from KISTI is acknowledged.

DOI: 10.1021/cs501600x
ACS Catal. 2015, 5, 965−971

REFERENCES

(1) Lewis, N. S.; Nocera, D. G. *Proc. Natl. Acad. Sci. U.S.A.* **2006**, *103*, 15729−15735.
(2) Olah, G. A.; Goeppert, A.; Prakash, G. S. *J. Org. Chem.* **2008**, *74*, 487−498.
(3) Qiao, J.; Liu, Y.; Hong, F.; Zhang, J. *Chem. Soc. Rev.* **2014**, *43*, 631−675.
(4) Lim, R. J.; Xie, M.; Sk, M. A.; Lee, J.-M.; Fisher, A.; Wang, X.; Lim, K. H. *Catal. Today* **2014**, *233*, 169−180.
(5) Gattrell, M.; Gupta, N.; Co, A. *Energy Convers. Manage.* **2007**, *48*, 1255−1265.
(6) Costentin, C.; Robert, M.; Saveant, J.-M. *Chem. Soc. Rev.* **2013**, *42*, 2423−2436.
(7) Kuhl, K. P.; Cave, E. R.; Abram, D. N.; Jaramillo, T. F. *Energy Environ. Sci.* **2012**, *5*, 7050−7059.
(8) Hori, Y.; Murata, A.; Takahashi, R. *J. Chem. Soc., Faraday Trans. 1* **1989**, *85*, 2309−2326.
(9) Hori, Y.; Wakebe, H.; Tsukamoto, T.; Koga, O. *Electrochim. Acta* **1994**, *39*, 1833−1839.
(10) Bromberg, L.; Cohn, D. *Heavy Duty Vehicles Using Clean, High Efficiency Alcohol Engines*; PSFC/JA-10-43; MIT Plasma Science & Fusion Center: Cambridge, MA, November, 2010.
(11) Goeppert, A.; Czaun, M.; Jones, J.-P.; Prakash, G. S.; Olah, G. A. *Chem. Soc. Rev.* **2014**, *43*, 7995−8048.
(12) Cheng, W.-H.; Kung, H. H.; *Methanol Production and Use*; CRC Press: New York, 1994;.
(13) Frese, K. W., Jr; Leach, S. C.; Summers, D. P. *Electrochemical Reduction of Aqueous Carbon Dioxide to Methanol*. Patent 4609441, Dec 18, 1986.
(14) Peterson, A. A.; Nørskov, J. K. *J. Phys. Chem. Lett.* **2012**, *3*, 251−258.
(15) Chan, K.; Tsai, C.; Hansen, H. A.; Nørskov, J. K. *ChemCatChem* **2014**, *6*, 1899−1905.
(16) Karamad, M.; Tripkovic, V.; Rossmeisl, J. *ACS Catal.* **2014**, *4*, 2268−2273.
(17) Lim, D.-H.; Jo, J. H.; Shin, D. Y.; Wilcox, J.; Ham, H. C.; Nam, S.-W. *Nanoscale* **2014**, *6*, 5087−5092.
(18) Hori, Y.; Electrochemical CO_2 Reduction on Metal Electrodes. *Modern Aspects of Electrochemistry*; Springer: New York, 2008; *42*, 89−189.
(19) Schouten, K. J. P.; Qin, Z.; Gallent, E. P. R.; Koper, M. T. *J. Am. Chem. Soc.* **2012**, *134*, 9864−9867.
(20) Hori, Y.; Wakebe, H.; Tsukamoto, T.; Koga, O. *Surf. Sci.* **1995**, *335*, 258−263.
(21) Durand, W. J.; Peterson, A. A.; Studt, F.; Abild-Pedersen, F.; Nørskov, J. K. *Surf. Sci.* **2011**, *605*, 1354−1359.
(22) Peterson, A. A.; Abild-Pedersen, F.; Studt, F.; Rossmeisl, J.; Nørskov, J. K. *Energy Environ. Sci.* **2010**, *3*, 1311−1315.
(23) Schouten, K.; Kwon, Y.; Van der Ham, C.; Qin, Z.; Koper, M. *Chem. Sci.* **2011**, *2*, 1902−1909.
(24) Greeley, J.; Mavrikakis, M. *Nat. Mater.* **2004**, *3*, 810−815.
(25) Bandarenka, A. S.; Varela, A. S.; Karamad, M.; Calle-Vallejo, F.; Bech, L.; Perez-Alonso, F. J.; Rossmeisl, J.; Stephens, I. E.; Chorkendorff, I. *Angew. Chem., Int. Ed.* **2012**, *51*, 11845−11848.
(26) Varela, A. S.; Schlaup, C. G.; Jovanov, Z. P.; Malacrida, P.; Horch, S.; Stephens, I. E. L.; Chorkendorff, I. *J. Phys. Chem. C* **2013**, *117*, 20500−20508.
(27) Hohenberg, P.; Kohn, W. *Phys. Rev.* **1964**, *136*, B864.
(28) Kresse, G.; Joubert, D. *Phys. Rev. B* **1999**, *59*, 1758.
(29) Kresse, G.; Furthmüller, J. *Comput. Mater. Sci.* **1996**, *6*, 15−50.
(30) Perdew, J. P.; Burke, K.; Ernzerhof, M. *Phys. Rev. Lett.* **1996**, *77*, 3865.
(31) Hammer, B.; Hansen, L. B.; Nørskov, J. K. *Phys. Rev. B* **1999**, *59*, 7413.
(32) Blöchl, P. E. *Phys. Rev. B* **1994**, *50*, 17953.
(33) Monkhorst, H. J.; Pack, J. D. *Phys. Rev. B* **1976**, *13*, 5188−5192.
(34) Nørskov, J. K.; Rossmeisl, J.; Logadottir, A.; Lindqvist, L.; Kitchin, J. R.; Bligaard, T.; Jonsson, H. *J. Phys. Chem. B* **2004**, *108*, 17886−17892.
(35) Rossmeisl, J.; Greeley, J.; Karlberg, G.; Electrocatalysis and Catalyst Screening from Density Functional Theory Calculations. *Fuel Cell Catalysis: A Surface Science Approach*; Wiley: Hoboken, NJ, 2009; Chapter 3, pp 57−92.
(36) Karlberg, G.; Wahnström, G. *Phys. Rev. Lett.* **2004**, *92*, 136103.
(37) Tripković, V.; Skúlason, E.; Siahrostami, S.; Nørskov, J. K.; Rossmeisl, J. *Electrochim. Acta* **2010**, *55*, 7975−7981.
(38) Yim, W.-L.; Johnson, J. K. *J. Phys. Chem. C* **2009**, *113*, 17636−17642.
(39) Desai, S. K.; Neurock, M. *Phys. Rev. B* **2003**, *68*, 075420.
(40) Evans, M.; Warhurst, E. *Trans. Faraday Soc.* **1938**, *34*, 614−624.
(41) Pallassana, V.; Neurock, M. *J. Phys. Chem. B* **2000**, *104*, 9449−9459.
(42) Liu, Z.-P.; Hu, P. *J. Chem. Phys.* **2001**, *115*, 4977−4980.
(43) Greeley, J.; Jaramillo, T. F.; Bonde, J.; Chorkendorff, I.; Nørskov, J. K. *Nat. Mater.* **2006**, *5*, 909−913.
(44) Man, I. C.; Su, H. Y.; Calle-Vallejo, F.; Hansen, H. A.; Martínez, J. I.; Inoglu, N. G.; Kitchin, J.; Jaramillo, T. F.; Nørskov, J. K.; Rossmeisl, J. *ChemCatChem* **2011**, *3*, 1159−1165.
(45) Siahrostami, S.; Verdaguer-Casadevall, A.; Karamad, M.; Deiana, D.; Malacrida, P.; Wickman, B.; Escudero-Escribano, M.; Paoli, E. A.; Frydendal, R.; Hansen, T. W. *Nat. Mater.* **2013**, *12*, 1137−1143.
(46) Nørskov, J. K.; Bligaard, T.; Logadottir, A.; Kitchin, J.; Chen, J.; Pandelov, S.; Stimming, U. J. *Electrochim. Acta* **2005**, *152*, J23−J26.
(47) Fernández, E. M.; Moses, P. G.; Toftelund, A.; Hansen, H. A.; Martínez, J. I.; Abild-Pedersen, F.; Kleis, J.; Hinnemann, B.; Rossmeisl, J.; Bligaard, T. *Angew. Chem., Int. Ed.* **2008**, *47*, 4683−4686.
(48) Abild-Pedersen, F.; Greeley, J.; Studt, F.; Rossmeisl, J.; Munter, T.; Moses, P. G.; Skulason, E.; Bligaard, T.; Nørskov, J. K. *Phys. Rev. Lett.* **2007**, *99*, 016105.
(49) Falsig, H.; Hvolbæk, B.; Kristensen, I. S.; Jiang, T.; Bligaard, T.; Christensen, C. H.; Nørskov, J. K. *Angew. Chem.* **2008**, *120*, 4913−4917.
(50) Tripkovic, V.; Vanin, M.; Karamad, M.; Björketun, M. R. E.; Jacobsen, K. W.; Thygesen, K. S.; Rossmeisl, J. *J. Phys. Chem. C* **2013**, *117*, 9187−9195.
(51) Greeley, J.; Nørskov, J. K.; Kibler, L. A.; El-Aziz, A. M.; Kolb, D. M. *ChemPhysChem* **2006**, *7*, 1032−1035.
(52) Hansen, H. A.; Montoya, J. H.; Zhang, Y.-J.; Shi, C.; Peterson, A. A.; Nørskov, J. K. *Catal. Lett.* **2013**, *143*, 631−635.

DOI: 10.1021/cs501600x
ACS Catal. 2015, 5, 965−971